Endothelin-2 deficiency causes growth retardation, hypothermia, and emphysema in mice

Inik Chang,[1] Alexa N. Bramall,[2,3] Amy Greenstein Baynash,[1] Amir Rattner,[4] Dinesh Rakheja,[5,6] Martin Post,[7,8,9,10] Stephen Joza,[7,8] Colin McKerlie,[7,8] Duncan J. Stewart,[11] Roderick R. McInnes,[2,3,12] and Masashi Yanagisawa[1,13,14]

[1]Department of Molecular Genetics, University of Texas Southwestern Medical Center, Dallas, Texas, USA. [2]Program in Developmental Biology, The Research Institute, The Hospital for Sick Children, Toronto, Ontario, Canada. [3]Department of Molecular Genetics, University of Toronto, Toronto, Ontario, Canada. [4]Department of Molecular Biology and Genetics, Johns Hopkins University School of Medicine, Baltimore, Maryland, USA. [5]Department of Pathology and [6]Children's Medical Center, University of Texas Southwestern Medical Center, Dallas, Texas, USA. [7]Program in Physiology and Experimental Medicine, The Research Institute, The Hospital for Sick Children, Toronto, Ontario, Canada. [8]Department of Laboratory Medicine and Pathology, [9]Department of Pediatrics, and [10]Institute of Medical Science, University of Toronto, Toronto, Ontario, Canada. [11]The Ottawa Hospital Research Institute and The University of Ottawa, Ottawa, Ontario, Canada. [12]Lady Davis Research Institute, Jewish General Hospital, McGill University, Montreal, Canada. [13]Howard Hughes Medical Institute, University of Texas Southwestern Medical Center, Dallas, Texas, USA. [14]International Institute for Integrative Sleep Medicine (WPI-IIIS), University of Tsukuba, Tsukuba, Japan.

To explore the physiological functions of endothelin-2 (ET-2), we generated gene-targeted mouse models. Global *Et2* knockout mice exhibited severe growth retardation and juvenile lethality. Despite normal milk intake, they suffered from internal starvation characterized by hypoglycemia, ketonemia, and increased levels of starvation-induced genes. Although ET-2 is abundantly expressed in the gastrointestinal tract, the intestine was morphologically and functionally normal. Moreover, intestinal epithelium–specific *Et2* knockout mice showed no abnormalities in growth and survival. Global *Et2* knockout mice were also profoundly hypothermic. Housing *Et2* knockout mice in a warm environment significantly extended their median lifespan. However, neuron-specific *Et2* knockout mice displayed a normal core body temperature. Low levels of *Et2* mRNA were also detected in the lung, with transient increases soon after birth. The lungs of *Et2* knockout mice showed emphysematous structural changes with an increase in total lung capacity, resulting in chronic hypoxemia, hypercapnia, and increased erythropoietin synthesis. Finally, systemically inducible ET-2 deficiency in neonatal and adult mice fully reproduced the phenotype previously observed in global *Et2* knockout mice. Together, these findings reveal that ET-2 is critical for the growth and survival of postnatal mice and plays important roles in energy homeostasis, thermoregulation, and the maintenance of lung morphology and function.

Introduction

The endothelin (ET) system comprises three 21-residue active peptides (ET-1, -2, and -3), two G protein–coupled receptors (ET_A and ET_B), and activating peptidases including the ET-converting enzymes (ECE-1 and -2) (1). The developmental and (patho)physiological roles of the ET system components have been extensively studied using gene-targeted mice. The ET-1/ECE-1/ET_A pathway is essential for the development of pharyngeal arch–derived, craniofacial, and cardiac tissues (2, 3), whereas the ET-3/ECE-1/ET_B pathway is essential for the development of the enteric nervous system and skin melanocytes (4, 5). Although *Ece-2*–null mice revealed no marked abnormalities (6), *Ece-1/Ece-2* double mutants exhibited more severe cardiac abnormalities, including endocardial cushion defects (7). These molecular genetic studies point to the highly local action of ETs. For example, although ET-1 (which is produced by vascular endothelial cells and other cell types) is distributed widely in all tissues, the peptide cannot prevent the phenotype of ET-3 deficiency, indicating that ET-3 produced in the immediate vicinity of the relevant target cells (i.e., enteric neuroblasts expressing the ET_B receptor) is essential.

In addition, specific roles of the ET system in heart and kidney have been investigated using the Cre/loxP system. Although cardiomyocyte-specific ET-1 mediates cardiac hypertrophy induced by thyroid hormone (8), the ET_A receptor is not necessary for either basal cardiac function or stress-induced response to angiotensin II or isoproterenol (9). Collecting duct–specific inactivation of ET-1 (10), ET_A receptor (11), ET_B receptor (12), as well as both ET_A and ET_B receptors (13) revealed the importance of the ET system in maintaining blood pressure and regulating sodium excretion.

Unlike other components of the ET system, very little is known about the biological function of endogenous ET-2. Although ET-2 is pharmacologically indistinguishable from ET-1, with equally high affinities for both ET_A and ET_B receptors, the tissue distribution of ET-2 is highly limited; ET-2 is most abundantly expressed in the intestine, suggesting a role in the gastrointestinal tract. Recently, a specific expression pattern of ET-2 in intestine and its possible roles in the maintenance of villous architecture have been hypothesized (14). In addition, several other potential roles of ET-2 have been proposed. *Et2* mRNA is strongly induced in photoreceptor cells in retinal diseases and injury, which may function as a stress signal to Muller cells through ET_B (15). ET-2 is produced by microglia and macrophages in the early stages of a mouse glaucoma model, which suggests a novel link between

Conflict of interest: The authors have declared that no conflict of interest exists.
Citation for this article: *J Clin Invest.* 2013;123(6):2643–2653. doi:10.1172/JCI66735.

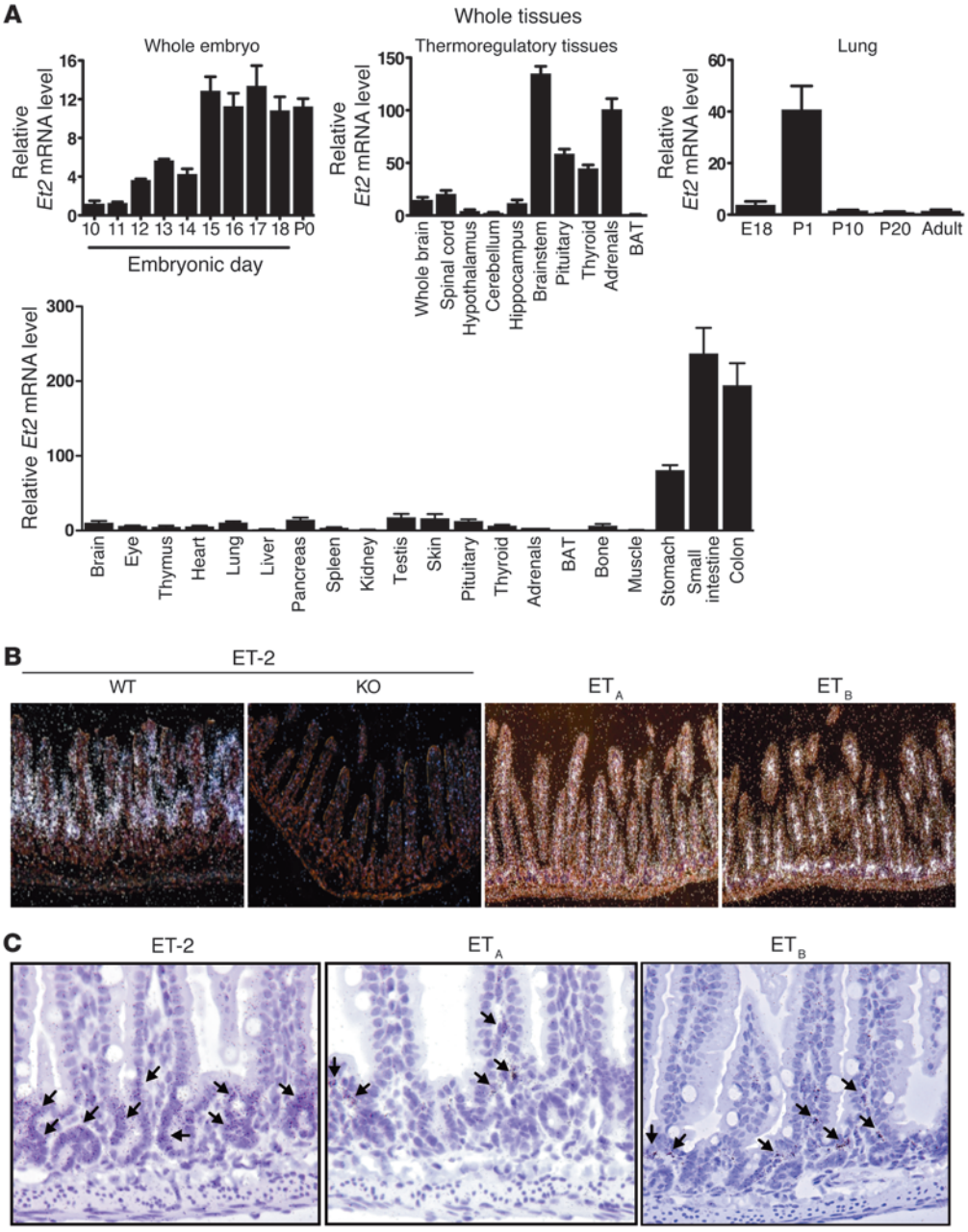

Figure 1
Expression profile of *Et2* mRNA. (**A**) qRT-PCR analysis of *Et2* mRNA expression in individual tissues and time course in the embryo and lung (n = 5). Values are presented as fold change relative to ET-2 expression in E10 (whole embryo), BAT (thermoregulatory tissues), P20 (lung), and muscle (whole tissues). (**B** and **C**) Localization of ET-2, ET_A, and ET_B in small intestine. In situ hybridization was performed with ^{35}S-labeled probes in the mouse ileum. (**B**) Representative photographs shown by dark-field microscopic imaging. Original magnification, ×20. Constitutive *Et2*-null mouse (KO) was used as a negative control. (**C**) Representative photographs shown by bright-field microscopic imaging. Original magnification, ×40. Black dots indicate the localization of genes, and arrows show specific localization of ET-2 in the villous and crypt epithelium, and ET_A and ET_B in the lamina propria.

microglia/macrophages and vascular dysfunction in glaucoma (16). During the ovulatory process, ET-2 is transiently produced in granulosa cells of the preovulatory follicles and induces follicular rupture through the ET_A receptor (17). In the field of tumor biology, ET-2 may serve as a marker for uveal melanoma (18) and is highly induced by hypoxia in squamous carcinoma cell lines derived from pharynx and cervix (19). ET-2 may also act as a chemoattractant for macrophages in tumors (20) and as an inducer of invasion (21) and a survival factor for breast tumor cells (22). ET-2 expression is upregulated in the early-stage clear cell subtype of renal cell carcinoma, suggesting a putative role in clear cell renal cell carcinoma progression (23).

In order to directly assess the in vivo role of ET-2 in mice, we generated constitutive and conditional *Et2*-deficient strains and comprehensively analyzed the phenotypes. The results reveal multiple essential roles of ET-2 in the growth and survival of postnatal mice.

Results

Tissue distribution of Et2 mRNA. ETs function as highly local and paracrine/autocrine mediators (1). Therefore, identification of ET-2–expressing tissues and cell types is critical to understanding its physiological function. As previously reported (24), *Et2* mRNA is abundantly expressed in the upper and lower gastrointestinal tract (Figure 1A). *Et2* is also detected at lower levels in a number of tissues including the brain, lung, pancreas, testis, and ovary. During the embryonic period, *Et2* mRNA expression is markedly increased from E15 and remains roughly constant until birth

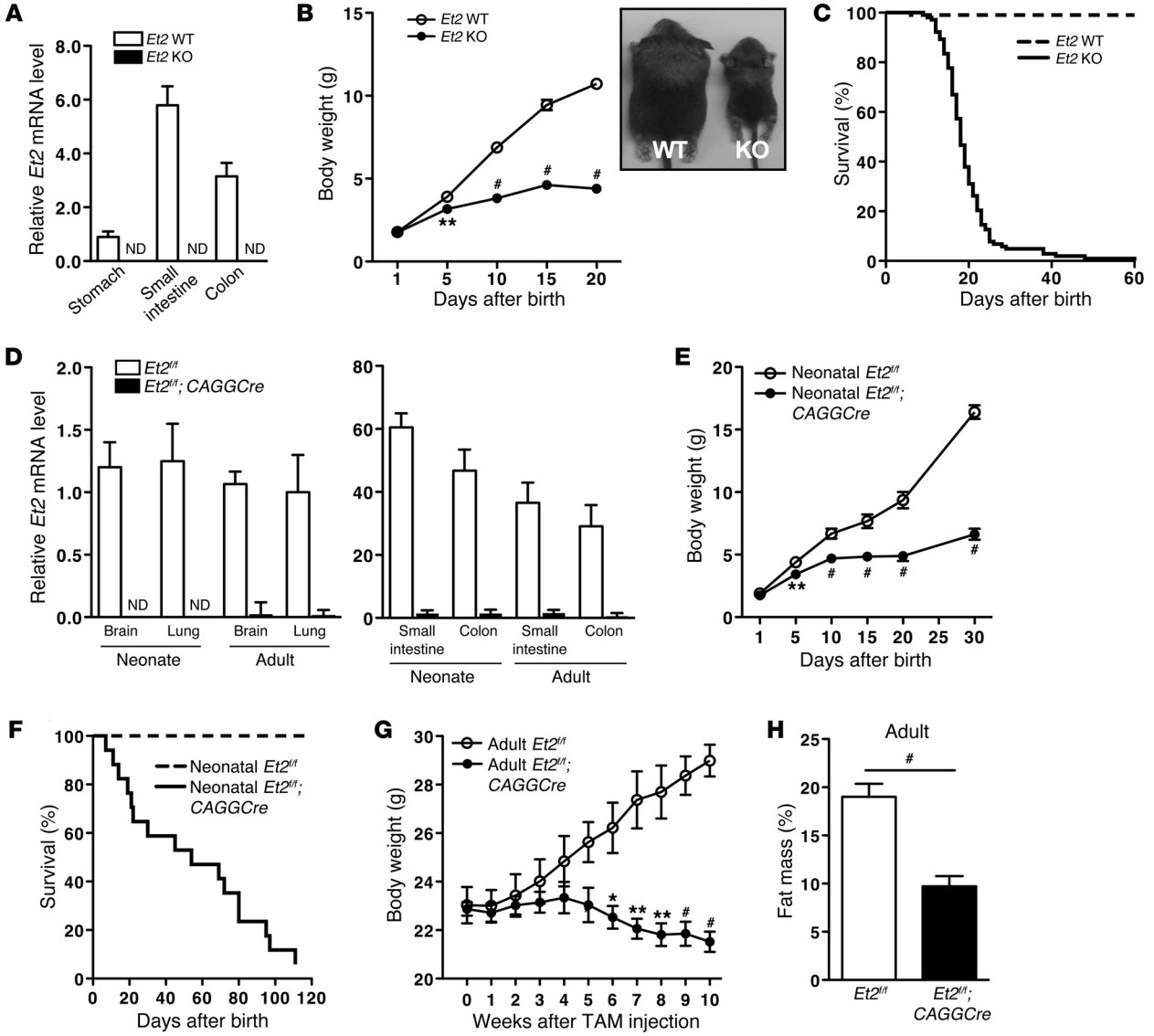

Figure 2

Essential role of ET-2 in growth and survival of postnatal mice. (**A**) qRT-PCR analysis demonstrating an absence of *Et2* mRNA in individual tissues of constitutive *Et2*-null mice ($n = 5$). Values are presented as fold change relative to ET-2 expression in stomach from WT mice. (**B**) Body weight during pre-weaning period of constitutive *Et2*-null and littermate WT mice ($n = 15$). Inset shows a representative photograph of *Et2*-null (right) and WT (left) mice at 2 weeks of age. (**C**) Survival ratio of constitutive *Et2*-null and littermate WT mice ($n = 100$–102). (**D**) qRT-PCR analysis demonstrating an absence of *Et2* mRNA level in individual tissues of neonatal and adult *Et2$^{f/f}$;CAGGCre-ER^{TM}* mice ($n = 5$). Values are presented as fold change relative to ET-2 expression in lung from adult *Et2$^{f/f}$* control mice. ND, not detected. (**E** and **F**) Body weight (**E**) and survival ratio (**F**) of neonatal *Et2$^{f/f}$;CAGGCre-ER^{TM}* and littermate control *Et2$^{f/f}$* mice ($n = 9$–17). (**G**) Body weight of adult *Et2$^{f/f}$;CAGGCre-ER^{TM}* and control littermate *Et2$^{f/f}$* mice ($n = 9$–10). (**H**) Fat content of adult *Et2$^{f/f}$;CAGGCre-ER^{TM}* and littermate control *Et2$^{f/f}$* mice after 10 weeks of tamoxifen (TAM) injection ($n = 9$–10). $^{*}P < 0.05$; $^{**}P < 0.01$; $^{\#}P < 0.001$.

(Figure 1A, whole embryo). Intestinal ET-2 is responsible for most *Et2* expression in the whole embryo at E15 (Supplemental Figure 1; supplemental material available online with this article; doi:10.1172/JCI66735DS1). *Et2* mRNA is also present in thermoregulatory tissues such as brainstem, spinal cord, pituitary, adrenals, and thyroid at low but detectable levels (Figure 1A; thermoregulatory tissues). In the lung, *Et2* mRNA is transiently and markedly increased shortly after birth (Figure 1A; lung). In situ hybridization in the ileum of the small intestine revealed that *Et2* mRNA is specifically expressed in the villous and crypt epithelium. In contrast, the *Eta* and *Etb* receptor mRNAs are located in the lamina propria below the epithelium (Figure 1, B and C).

ET-2 is essential for the growth and survival of postnatal mice. Constitutive *Et2*-null mice were generated by replacing a portion of exon 1 and all of exon 2 encoding the mature ET-2 peptide with the neo cassette (Supplemental Figure 2A). The absence of *Et2* mRNA was confirmed by quantitative RT-PCR (qRT-PCR) because ET-2 is immunologically indistinguishable from ET-1 (Figure 2A). Constitutively *Et2*-null mice were born healthy with expected Mendelian frequencies. Out of 154 pups examined, there were 40

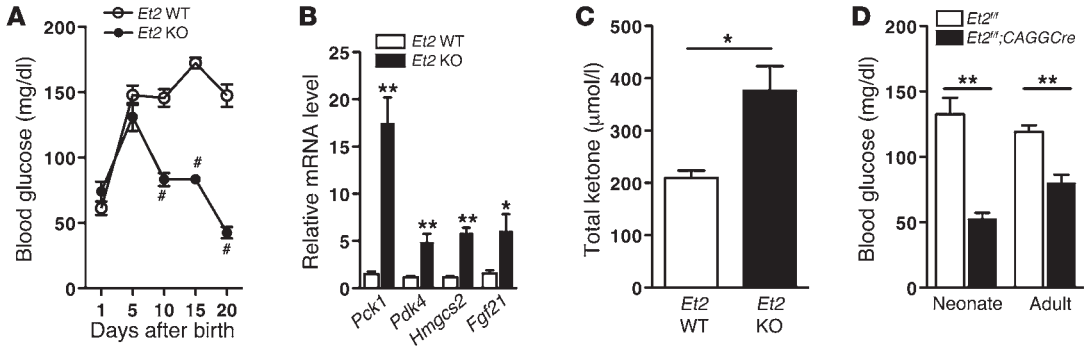

Figure 3

Internally starved state of *Et2*-null mice. (**A**) Blood glucose levels of constitutive *Et2*-null and littermate WT mice at the indicated age (n = 10). (**B**) Expression of starvation-induced genes in constitutive *Et2*-null and littermate WT mice at 2 weeks of age. qRT-PCR was performed using mRNAs extracted from liver (n = 4). Values are presented as fold change relative to ET-2 expression in WT control mice. (**C**) Serum total ketone levels of constitutive *Et2*-null and littermate WT mice at 2 weeks of age (n = 4). (**D**) Blood glucose levels of neonatal *Et2$^{f/f}$;CAGGCre-ER^{TM}* (2-week-old), adult *Et2$^{f/f}$;CAGGCre-ER^{TM}* (6-week-old) and their littermate control *Et2$^{f/f}$* mice (n = 10). $^{*}P < 0.05$; $^{**}P < 0.01$; $^{\#}P < 0.001$.

(26.0%) *Et2$^{+/+}$*, 72 (52.6%) *Et2$^{+/-}$*, and 42 (27.2%) *Et2$^{-/-}$* mice. At P3, the appearance and size of the *Et2*-null pups were similar to their WT littermates. Although *Et2*-null pups were frequently observed being nursed and normal amounts of milk were found in the stomach (Supplemental Figure 3), by P5, *Et2*-null mice failed to thrive and displayed severe growth retardation (Figure 2B). The mutant mice eventually died by 3 to 4 weeks of age (Figure 2C).

Despite the obvious postnatal phenotype of constitutive *Et2*-null mice, ET-2 expression is increased from E15 (Figure 1A). Hence, to examine when the presence of ET-2 is important for growth and survival between the embryonic and postnatal periods, we generated systemically inducible *Et2*-null mice by crossing mice with *loxP*-flanked ET-2 (*Et2$^{f/f}$*) (Supplemental Figure 2B) with mice harboring Cre-ER^{TM} recombinase driven by a chimeric promoter of the cytomegalovirus immediate-early enhancer and chicken β-actin promoter/enhancer (CAGG) (25). Reduced expression of *Et2* mRNA in *Et2$^{f/f}$;CAGGCre-ER^{TM}* mice on P0 by gavage feeding of tamoxifen to the dam (neonatal *Et2$^{f/f}$;CAGGCre-ER^{TM}*) or at 6 weeks of age following intraperitoneal injection of tamoxifen (adult *Et2$^{f/f}$;CAGGCre-ER^{TM}*) was confirmed by qRT-PCR in the brain, lung, small intestine, and colon (Figure 2D). Neonatal *Et2$^{f/f}$;CAGGCre-ER^{TM}* mice fully recapitulated the phenotype of constitutive null mice: growth retardation (Figure 2E) and early lethality (Figure 2F). Adult *Et2$^{f/f}$;CAGGCre-ER^{TM}* mice also showed diminished weight gain (Figure 2G). Fat mass of adult *Et2$^{f/f}$;CAGGCre-ER^{TM}* mice was consistently decreased after 10 weeks of ET-2 inactivation (Figure 2H), although removal of ET-2 in the adult did not cause early lethality. Taken together, these results indicate that ET-2 is essential for growth regulation and survival of postnatal mice and the maintenance of energy homeostasis even in adulthood.

Et2-null mice are internally starved. To gain insight into the mechanism of this intriguing phenotype, we analyzed blood parameters of constitutive *Et2*-null mice at the age of 2 weeks. Overall, there was no significant difference between the genotypes. However, blood glucose levels were strikingly low in *Et2*-null mice under the fed condition (Supplemental Table 1), and this was maintained at all ages (Figure 3A). Blood urea nitrogen (BUN) and uric acid levels were significantly elevated, suggesting an increased catabolic response to energy deprivation (Supplemental Table 1). Despite the low blood glucose concentrations, insulin levels of *Et2*-null mice were not significantly different from those of WT controls and were normally regulated in both fed and fasted conditions (Supplemental Figure 4A). Although mild, T3 levels were reduced in the mutant mice, implicating a decreased metabolic rate for these animals (Supplemental Figure 4B). Since thyroid hormone is important in maintaining the basal level of metabolism and neonatal growth, we attempted to rescue the abnormal growth and survival of *Et2*-null mice by thyroid hormone replacement. Neither growth retardation nor early lethality was improved, however, by T3 supplementation (Supplemental Figure 5).

The results of normal milk consumption (Supplemental Figure 3) and blood chemistry (Supplemental Table 1) indicate that constitutive *Et2*-null mice suffered from apparent internal starvation. In order to verify this, we measured the expression of genes known to be induced by starvation. As expected, mRNA expression of phosphoenolpyruvate carboxykinase 1 (*Pck1*) and pyruvate dehydrogenase kinase isozyme 4 (*Pdk4*), key gluconeogenic enzymes, was upregulated in the liver of *Et2*-null mice (Figure 3B). Expression of hydroxymethylglutaryl-CoA synthase 2 (*Hmgcs2*), which catalyzes a key step in ketone body synthesis (Figure 3B), and the concentration of serum total ketone bodies were also elevated in *Et2*-null mice compared with WT mice (Figure 3C). Furthermore, expression of fibroblast growth factor 21 (*Fgf21*), which was recently discovered as a key regulator of the body's adaptation to fasting (26), was significantly induced in the liver of constitutive *Et2*-null mice (Figure 3B). Neonatal and adult *Et2$^{f/f}$;CAGGCre-ER^{TM}* mice also exhibited significantly lower blood glucose levels than the controls (Figure 3D). These data suggest that ET-2 deficiency contributes to an internally starved state in mice, and this may be the critical underlying mechanism for the growth retardation and early lethality of *Et2*-null mice.

Intestinal ET-2 is not essential for growth regulation and survival of mice. The internally starved phenotype, abundant expression of *Et2* mRNA in the gut, and local activity of ET strongly support a hypothesis by which intestinal dysfunction leading to malabsorption and/or malnutrition could cause the internally starved state of the *Et2*-null mice. To test this hypothesis, we first examined nutrient management. We found that fat absorption, measured by the amount of [^{3}H] triolein present in the small intestine and its

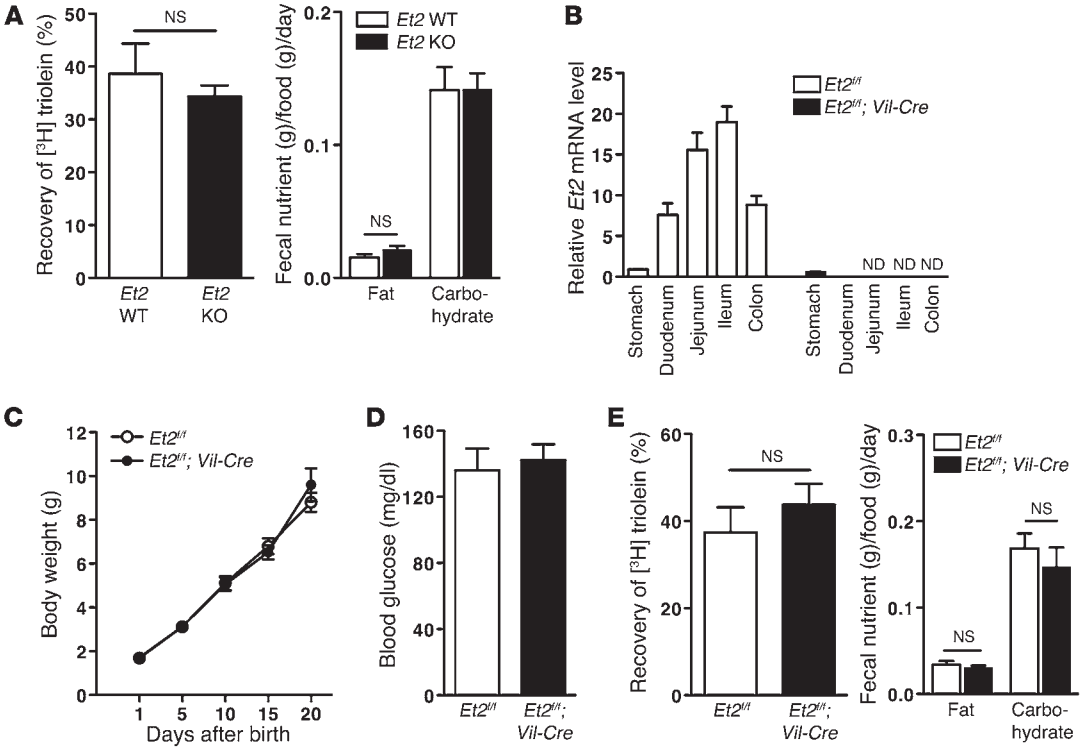

Figure 4

No detectable abnormalities in energy-related processes of constitutive and intestinal epithelium–specific *Et2*-null mice. (**A**) Dietary fat absorption (left) and excretion of fats and carbohydrates (right) of 6-week-old "rescued" constitutive *Et2*-null and littermate WT mice (n = 5). (**B**) qRT-PCR analysis demonstrating intestine-specific deletion of *Et2* by villin promoter–driven Cre recombinase (n = 5). Values are presented as fold change relative to ET-2 expression in stomach from control $Et2^{f/f}$ mice. (**C**) Body weight of $Et2^{f/f}$*;Vil-Cre* and their littermate control $Et2^{f/f}$ mice (n = 21–23). (**D**) Blood glucose levels of $Et2^{f/f}$*;Vil-Cre* and their littermate control $Et2^{f/f}$ mice at 2 weeks of age (n = 10). (**E**) Dietary fat absorption (left) and excretion of fats and carbohydrates (right) of 6-week-old $Et2^{f/f}$*;Vil-Cre* mice and their littermate controls (n = 5). ND, not detected; NS, nonsignificant.

content after oral gavage, was similar in control and constitutive *Et2*-null mice (Figure 4A, left). In addition, the proportion of fat and carbohydrate in feces did not exhibit any apparent difference in *Et2*-null mice (Figure 4A, right). Finally, as measured by qRT-PCR, mRNA levels of genes responsible for digestion and absorption of fat, carbohydrate, and protein were not significantly altered in the intestines of constitutive *Et2*-null mice compared with WT controls (Supplemental Figure 6).

To directly address the role of enterocytic ET-2, we generated intestinal epithelium–specific *Et2*-null mice by crossing $Et2^{f/f}$ mice with mice carrying Cre recombinase driven by the villin (*Vil*) promoter (27). Intestinal epithelium–specific recombination of the *loxP* sites was verified by PCR with genomic DNA (Supplemental Figure 7), and loss of *Et2* mRNA expression was confirmed by qRT-PCR in different parts of the intestine (Figure 4B). The level of *Et2* mRNA was unchanged in other organs, including the stomach, since the villin promoter is inactive in the stomach as previously reported (ref. 27, Supplemental Figure 7, and Figure 4B). $Et2^{f/f}$*;Vil-Cre* mice were born healthy and, unlike the constitutive and inducible *Et2*-null mice, no defects in growth (Figure 4C) or blood glucose levels (Figure 4D) were observed. Moreover, as shown in constitutive *Et2*-null mice, neither fat absorption nor excretion of fats and carbohydrates in feces significantly changed in the $Et2^{f/f}$*;Vil-Cre* mice (Figure 4E). It is unlikely that ET-1 or ET-3 is compensating for the loss of ET-2, since the expression of *Et1* and *Et3* mRNA was unchanged in the small intestine of constitutive and intestinal epithelium–specific *Et2*-null mice (Supplemental Figure 8). Therefore, contrary to our original hypothesis that ET-2 may play an important role in the (patho)physiology of the intestine, these data reveal that the intestine is not an essential site of ET-2 action under normal physiological conditions.

Since stomach *Et2* mRNA expression is intact (Figure 4B and Supplemental Figure 7) and no significant abnormality was observed in $Et2^{f/f}$*;Vil-Cre* mice (Figure 4, C and D), it seemed plausible that pH and enzyme secretion in the stomach could be affected by global ET-2 deficiency. The pH of stomach content from constitutive *Et2*-null mice was more acidic (pH≈3–4) compared with WT controls (pH≈5–6), perhaps contributing to enhanced protein denaturation. Therefore, we first examined mRNA levels for key proteins regulating acidification, protein digestion, or milk coagulation in the stomach and found that the expression of these genes was not significantly different between stomach samples of WT and constitutive *Et2*-deficient mice (Supplemental Figure 9). To determine whether the abnormal growth rate is caused by the aberrant digestion and/or absorption of nutrients due to an altered stomach pH, we provided the mice with sodium bicarbonate in drinking water to neutralize the stomach pH. However, no improvement in lifespan of the constitutive *Et2*-null mice was observed (Supplemental Figure 10). Among the numerous ET-2–expressing tissues, *Et2* mRNA expression was detected in whole

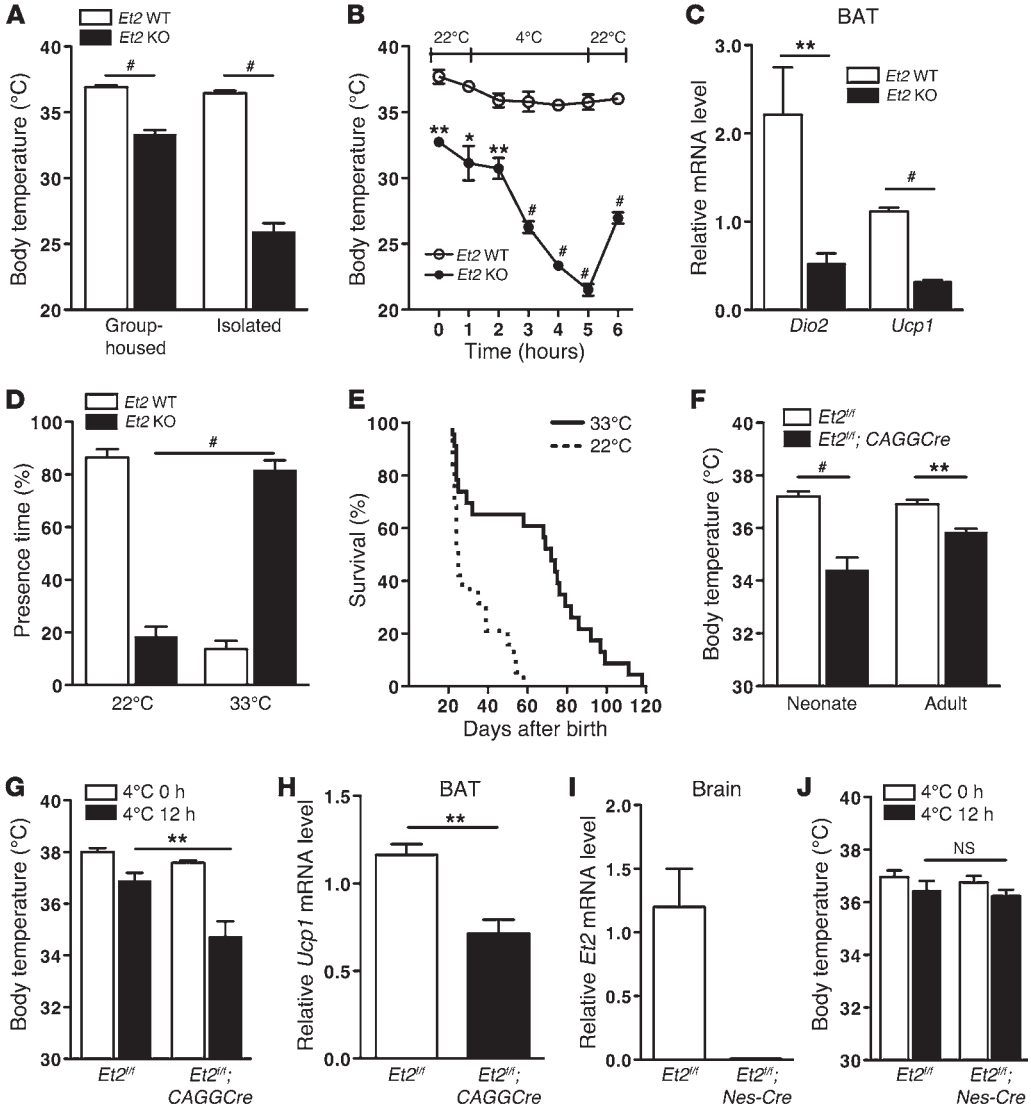

Figure 5

Defective thermoregulation of *Et2*-null mice. (**A**) Core body temperature of group-housed and isolated 3-week-old constitutive *Et2*-null mice ($n = 10$). (**B**) Core body temperature of 6-week-old "rescued" constitutive *Et2*-null and littermate WT mice in cold environment ($n = 6$). (**C**) qRT-PCR of *Dio2* and *Ucp1* mRNA levels in BAT from 6-week-old "rescued" constitutive *Et2*-null and littermate WT mice after 5 hours of cold exposure ($n = 4$). Values are presented as fold change relative to ET-2 expression in control WT mice. (**D**) Temperature choice test of 6-week-old "rescued" constitutive *Et2*-null and littermate WT mice ($n = 14–21$). (**E**) Survival ratio of constitutive *Et2*-null mice housed in warm (33°C) and ambient (22°C) environment from 3 weeks of age ($n = 20–21$). (**F**) Core body temperature of neonatal (2-week-old) and adult *Et2$^{f/f}$;CAGGCre-ER^{TM}* (6-week-old) mice, and littermate control *Et2$^{f/f}$* mice at ambient temperature ($n = 7–10$). (**G**) Core body temperature of adult *Et2$^{f/f}$;CAGGCre-ER^{TM}* and control mice in a cold environment at 6 weeks of age ($n = 10$). (**H**) qRT-PCR of *Ucp1* mRNA levels in BAT from adult *Et2$^{f/f}$;CAGGCre-ER^{TM}* and littermate control *Et2$^{f/f}$* mice after 12 hours of cold exposure ($n = 4$). (**I**) qRT-PCR analysis demonstrating brain-specific deletion of *Et2* by nestin promoter-driven Cre recombinase. (**J**) Core body temperature of *Et2$^{f/f}$;Nes-Cre* and littermate control *Et2$^{f/f}$* mice at 6 weeks of age ($n = 5$). $^{*}P < 0.05$; $^{**}P < 0.01$; $^{\#}P < 0.001$.

pancreas, albeit at relatively low levels (Figure 1A; whole tissues). Because insulin secretion is normal in constitutive *Et2*-null mice (Supplemental Figure 4A), we analyzed the expression of exocrine pancreatic enzymes. However, mRNA levels of genes involved in the digestion and absorption of fat, carbohydrate, and protein were not significantly changed in the constitutive *Et2*-null mice compared with the WT controls (Supplemental Figure 11).

Defective thermoregulation of Et2-null mice. Constitutive *Et2*-null mice exhibited mild hypothermia, which could be a consequence of internal starvation (Figure 5A; group-housed). When *Et2*-null mice were separated for 3 hours from the dam and siblings, the core body temperature of the *Et2*-null mice drastically declined to 25.9 ± 0.6°C (versus 36.5 ± 0.2°C for the WT controls) at room temperature (Figure 5A; isolated). Thus, we exposed constitutive *Et2*-null mice to a cold environment to examine whether ET-2 is important for heat generation and conservation. Although the control mice maintained a body temperature within a 2.2°C range, the core body temperature of *Et2*-null mice dropped to approximately 22°C within 5 hours of exposure to 4°C (Figure 5B). Type 2 iodothyrosine deiodinase (DIO2) is activated during cold stress to increase triiodothyroine (T3) concentration in brown adipose tissue (BAT) (28). The level of uncoupling protein 1 (UCP1), the key thermogenic regulator in BAT, is regulated by T3 (29). Therefore, we examined the expression of DIO2 and UCP1 to determine whether ET-2 deficiency affects these genes and leads to defects in thermogenesis. As expected, *Dio2* and *Ucp1* mRNA levels were significantly reduced in the BAT of cold-exposed constitutive *Et2*-null mice (Figure 5C). Histological analysis also revealed abnormalities, including reduced nuclei number and a marked accumulation of large lipid vacuoles, suggesting that there is no apparent increase in lipolysis to generate heat (Supplemental Figure 12). Low body temperature induces behavioral responses in mice, such as huddling in a

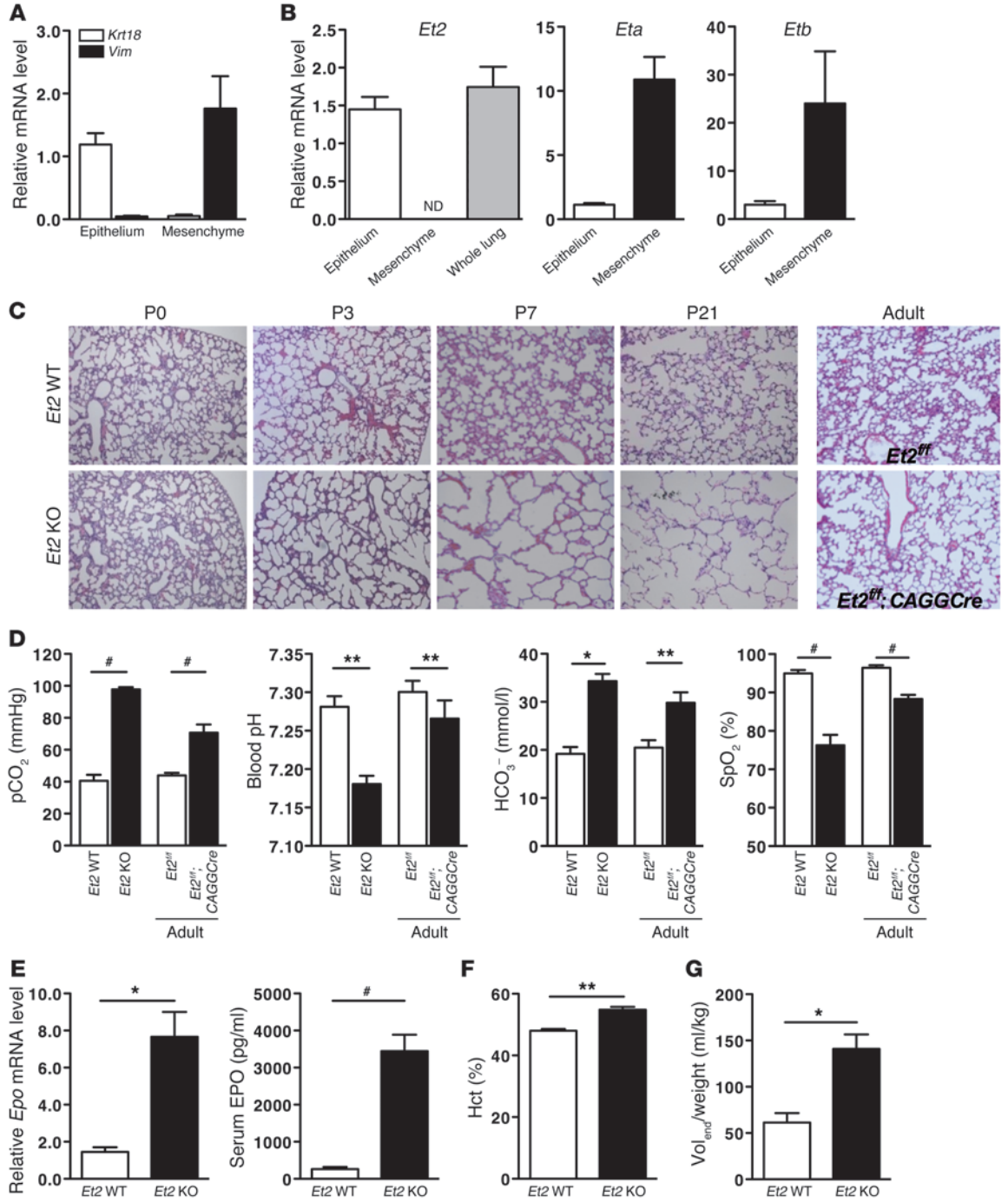

Figure 6

Impaired lung morphology and function of *Et2*-null mice. (**A** and **B**) qRT-PCR was performed using mRNAs extracted from isolated epithelial and mesenchymal cell populations of rat lung to examine the purity of cell fractions (**A**) and expression of ET-2, ET_A, and ET_B (**B**) (n = 3–5). Values are presented as fold change relative to gene expression in epithelium for *Krt18*, *Et2*, *Eta*, and *Etb*, and in mesenchyme for *Vim*. (**C**) Histological phenotypes of the lungs of *Et2*-null and littermate WT mice. Lung sections from constitutive *Et2*-null (P1-P21) and adult *Et2$^{f/f}$;CAGGCre-ER^{TM}* (8-week-old) mice and their control littermates were stained with H&E. Original magnification, ×10. (**D**) Blood gas of constitutive *Et2*-null (2-week-old) and adult *Et2$^{f/f}$;CAGGCre-ER^{TM}* (8-week-old) mice and their control littermates (n = 6). (**E**–**G**) Levels of erythropoietin (*Epo*) mRNA in kidneys (left) and protein in serum (right) (**E**), hematocrit (Hct) (**F**) level, and total lung capacity (**G**) of constitutive *Et2*-null and control littermate mice at 3 weeks of age (n = 5). $^{*}P < 0.05$; $^{**}P < 0.01$; $^{\#}P < 0.001$.

curled posture and seeking a warmer place. A stationary curled posture was notably seen in constitutive *Et2*-deficient mice. When WT and *Et2*-deficient mice were placed in an apparatus with 2 available thermal zones (22°C versus 33°C), there was an apparent difference in the amount of time spent in each zone. Unlike the cold-zone preference of WT mice, *Et2*-null mice clearly sought a warmer location (Figure 5D).

The thermoregulatory defect results of constitutive *Et2*-null mice led us to hypothesize that placing *Et2*-null mice at a higher ambient temperature might delay their premature death. To test this possibility, 1 group of 3-week-old constitutive *Et2*-null mice was housed at room temperature, while the second group was placed on a 33°C heating plate for added warmth. The *Et2*-null mice housed at the higher temperature lived significantly longer — in fact, median lifespan was extended from 4 weeks to 9 weeks (Figure 5E).

Consistent with global *Et2*-null mice, neonatal and adult *Et2$^{f/f}$;CAGGCre-ER^{TM}* mice were also mildly hypothermic at ambient temperature (Figure 5F). To examine whether ET-2 deficiency in adulthood is also important for heat generation and conservation, adult *Et2$^{f/f}$;CAGGCre-ER^{TM}* mice and their control littermates were challenged with a cold environment. Control *Et2$^{f/f}$* mice maintained their core body temperature within a 1.2°C range over a 12-hour period of cold exposure (38.0 ± 0.15°C versus 36.8 ± 0.31°C; Figure 5G). However, as shown in constitutive *Et2*-null mice, the core body temperature of adult *Et2$^{f/f}$;CAGGCre-ER^{TM}* mice significantly dropped after 12 hours of cold exposure (36.9 ± 0.3°C versus 34.7 ± 0.5°C; Figure 5G). Greater body weight (25 g) and a decreased surface/volume ratio may partially explain why hypothermia was not as extreme in adult *Et2$^{f/f}$;CAGGCre-ER^{TM}* mice compared with constitutive *Et2*-null mice (10 g, 6-week-old mice rescued from a warm environment). *Ucp1* mRNA levels in BAT from cold-exposed adult *Et2$^{f/f}$;CAGGCre-ER^{TM}* mice were also downregulated (Figure 5H).

ET-2 might be involved in central thermoregulation because: (a) despite the profound hypothermia, DIO2 and UCP1 expression is reduced in mutant mice (Figure 5C); (b) thermogenesis of BAT is activated by the hypothalamus via the sympathetic nervous system (30); and (c) *Et2* mRNA is present in the brainstem and spinal cord but not in BAT (Figure 1A; thermoregulatory tissues). To directly examine this possibility, we generated neuron-specific *Et2*-null mice by crossing *Et2$^{f/f}$* mice with mice carrying Cre recombinase driven by the nestin (*Nes*) promoter. Loss of *Et2* mRNA expression in the brain was verified by qRT-PCR (Figure 5I). *Et2$^{f/f}$;Nes-Cre* mice were born healthy, and no growth defects were observed (Supplemental Figure 13). Moreover, unlike constitutive *Et2*-null mice, the neuron-specific *Et2*-null mice displayed normal core body temperature (Figure 5J; 4°C at 0 hours), even in a cold environment (Figure 5J; 4°C at 12 hours). These results suggest that aberrant thermoregulation in constitutive *Et2*-null mice is not a result of the loss of ET-2 expression in the central nervous system.

Compromised lung morphology and function in Et2-deficient mice. We often observed breathing difficulties in constitutive *Et2*-null mice, with audible wheezing from the age of 1 week onward. Consistent with a previous report (31), we found that *Et2* mRNA is expressed at a low level in the lung and exhibits a transient increase at birth (Figure 1A; lung). In order to identify the ET-2–expressing cell types in the lung, we performed qRT-PCR using isolated epithelial and mesenchymal cell populations from rat lung (E19.5). The purity of the fractions was confirmed by qRT-PCR of cytokeratin-18 (*Krt18*) and vimentin (*Vim*) for epithelium and mesenchyme, respectively. Very low levels of *Vim* mRNA in the epithelial fraction reflect a minor contamination of fibroblasts (Figure 6A). Expression of *Et2* mRNA was only detected in the epithelial fraction. In contrast, the *Eta* and *Etb* mRNAs are predominantly expressed in the mesenchyme, possibly indicating a paracrine function for ET-2 in the lung (Figure 6B). The expression pattern strongly indicates that ET-2 might be involved in postnatal lung development and may mediate specific interactions between epithelial and mesenchymal cells.

Histological analyses of the lung displayed severe abnormalities in postnatal lung alveogenesis. The lungs of constitutive *Et2*-null mice exhibited enlarged air spaces with substantial simplification of lung alveolar structure compared, with WT controls (Figure 6C; P0-P21). Similar morphological changes were also observed in adult *Et2$^{f/f}$;CAGGCre-ER^{TM}* mice (Figure 6C; Adult). These data suggest that ET-2 is critical not only for postnatal lung development, but also for the maintenance of lung structure in adulthood.

To examine the physiological and functional relevance of these morphological abnormalities, we first examined blood gases. Partial pressure of carbon dioxide (pCO_2) was elevated in both constitutive *Et2*-null mice and adult *Et2$^{f/f}$;CAGGCre-ER^{TM}* mice. As a result of hypercapnia, blood pH was more acidic, and bicarbonate (HCO_3^-) levels were clearly elevated in both *Et2* mutant lines. The oxygen saturation percentage of arterial hemoglobin (SpO_2) in *Et2*-null mice was markedly decreased, revealing hypoxemia (Figure 6D). Consistent with the decrease in SpO_2, mRNA synthesis of erythropoietin (*Epo*) in the kidneys was induced. EPO protein levels in serum were significantly increased in the *Et2*-null mice (Figure 6E), likely resulting in an increase in plasma hematocrit (Figure 6F). As a consequence of altered structure, the lungs of *Et2*-null mice had larger total lung capacities compared with WT controls (Figure 6G). These results indicate that the morphological abnormalities of *Et2*-deficient lungs may lead to hypercapnia and hypoxemic hypoxia in *Et2*-null mice.

Discussion

In the present study, we explore the biological function of ET-2 using knockout mouse models. Mice with constitutive or systemically-induced deletion of ET-2 exhibited defective energy homeostasis, thermoregulation, and lung morphology and function. Our comprehensive analyses, including the examination of tissue-specific knockouts, show that intestinal and neuronal ET-2 is not fully accountable for the regulation of energy homeostasis and body temperature, respectively. The dramatic effects of ET-2 deficiency in the lung are newly discovered and the lung may therefore be an important site for critical ET-2 action. In the lung, *Et2* mRNA is expressed in epithelial cells and transiently increased soon after birth. Temporary induction of *Et2* mRNA by pathological or physiological stimuli is also observed in the photoreceptor cells of the retina (15) and the granulose cells of the ovary (17). The analysis of lung-specific *Et2*-deficient mice will help to determine whether ET-2 expression in the lung is critical for the growth regulation and survival of postnatal mice. Lung epithelium is composed of several specific cell types such as squamous alveolar (type I) and great alveolar (type II) cells in the alveolar epithelium, and ciliated cells and Clara cells in the respiratory bronchioles. Cell type–specific gene promoters expressing Cre are available for each lung epithelial cell population: surfactant protein C (SP-C) for type II cells, Clara cell secretory protein (CCSP) for Clara cells, and forkhead box J1 (Foxj1) for ciliated cells (32, 33). Future studies will be

needed to determine the specific epithelial cell population responsible for ET-2 expression and thus the most appropriate promoter for removal of ET-2 in the lung.

In this report, internal starvation, severe hypothermia, and lung dysfunction caused by ET-2 deficiency are proposed as possible independent underlying mechanisms explaining the growth retardation and early lethality of *Et2*-null mice. Nonetheless, it is highly possible that these phenotypes are not independent, since metabolic rate, body temperature, and breathing regulation are physiologically interrelated. First, starvation might be the primary abnormality caused by the absence of ET-2. Under the stressful environment imposed by reduced food availability and a low ambient temperature, small mammals, including mice, can enter torpor to conserve energy by dropping their body temperature to near-ambient temperature levels (34). Since nutritional availability is an important determinant of normal lung development, chronic nutrient restriction may induce structural and functional alterations in the lung (35). The lungs of rats starved soon after birth exhibit impaired alveolar development and enlarged air spaces consistent with the phenotype of *Et2*-null mice (36). Starvation or calorie restriction in adult animals including humans can also lead to structural and functional changes in the lung (37). Although the lung abnormalities were less marked than what was seen in the *Et2*-null mice, these studies raise the possibility that hypothermia and lung dysfunction might be a secondary effect of internal starvation due to ET-2 deficiency.

Another possibility is that lung dysfunction is the primary abnormality underlying the phenotype of *Et2*-deficient mice. PDGF-A signaling is a critical event in lung alveolar myofibroblast development and alveogenesis. The core fucosylation (α1, 6-fucosylation) of TGF-β1 receptors is crucial for the prevention of developmental and progressive/destructive emphysema. *Pdgfa* and α1, 6-fucosyltransferase–null (*Fut8*-null) mice display airspace enlargement with the failure of alveolar septation in the lung accompanied by postnatal growth retardation and early lethality (38, 39). Malnutrition and weight loss are common problems in chronic obstructive pulmonary disease (COPD) (40), and significant loss of body weight is also observed in mouse models exposed to hypoxia (41). Many studies have reported that hypoxia evokes a regulated decrease in body temperature (i.e., anapyrexia) as a compensatory response to decreased oxygen consumption (42). Chronic hypercapnia can impair thermoregulation by increasing sweating and reducing shivering in humans (43). Thus, it is quite reasonable to hypothesize that in *Et2*-null mice, an internally starved state and hypothermia are the consequence, and not the cause, of severe lung dysfunction and respiratory failure.

Whether or not the profound hypothermia of *Et2*-null mice is a byproduct of internal starvation and lung dysfunction, it is still an important contributor to the phenotype. Since *Et2*-null mice reared in warm conditions lived longer than their null littermates housed at room temperature (Figure 5F), abnormal thermoregulation may play a critical role in the premature death of *Et2*-null mice. In a cold environment, *Et2*-null mice are unable to maintain body temperature. Furthermore, hypothermia might not be the consequence of torpor, since the expression of pancreatic lipases was paradoxically decreased in the liver of *Et2*-null mice (Supplemental Figure 13), whereas an increase in expression is a hallmark of torpor (44, 45). Nonetheless, these results deserve cautious interpretation, and this hypothesis needs to be explored further, since loss of neuronal ET-2 does not cause defects in thermoregulation.

The apparent difference in survival between constitutive and systemically inducible *Et2*-null mice (Figure 2, C and F) may suggest the importance of ET-2 during embryonic development. However, it is highly possible that the less severe phenotype of inducible *Et2*-null mice results from the gradual recombination of the floxed *Et2* gene rather than the effect of ET-2 on embryonic development. Although the excision of the floxed gene can be induced relatively quickly, the efficiency still depends on time and is different in each individual (25). Therefore, the phenotype appearance resulting from the gene's absence will occur gradually. In our experimental setting, tamoxifen was provided to the dam after giving birth, and not during pregnancy. Therefore, the recombination efficiency of each *Et2$^{f/f}$;CAGGCre-ER^{TM}* pup will show big differences depending on its milk consumption. As shown in Supplemental Figure 15, six hours after birth, intestinal ET-2 is still expressed in some neonatal *Et2$^{f/f}$;CAGGCre-ER^{TM}* mice, but it is completely lost around 48 hours after birth. This result supports our hypothesis that ET-2 action in the postnatal period is essential for the growth and survival of the mice.

The results of our mouse genetic study of ET-2 provide insights into its potential implication and role in humans. In contrast to the intestine-restricted expression in rodents, human ET-2 expression has been detected in a range of tissues such as heart, lung, kidney, vasculature, ovary, and colon (46). Currently, ET receptor antagonists such as bosentan and ambrisentan are clinically used for the treatment of pulmonary arterial hypertension. However, our data showing the possible role of ET-2 in the maintenance of lung morphology and function suggest that blocking the ET-2 signaling pathway may have adverse effects in the lungs of human patients. Therefore, the effect of ET antagonists on normal lung morphology and basal function should be examined in preclinical safety tests in clinical trials. The beneficial effect of bosentan and Ro 48-5695 in the rat trinitrobenzene sulfonic acid–induced colitis model supports the possible use of ET receptor antagonists in the treatment of human inflammatory bowel disease (IBD) (47–49). However, a clear role of ET in IBD pathogenesis has not been conclusively established (50). Unlike in rats, ET-2 is the predominant ET isoform in both mouse (I. Chang et al., unpublished observations) and human colonic mucosa (50). Therefore, investigating a model of intestinal injury and inflammation with *Et2$^{f/f}$;Vil-Cre* mice would be informative to address the question of whether the beneficial effects of ET antagonists reported in the rat model are relevant to the treatment of human IBD.

Methods

Animal experiment. Detailed information regarding the generation of the constitutive and conditional *Et2* knockout mice is described in Supplemental Data and Supplemental Figure 1. Mice were housed in a temperature-controlled environment with 12-hour light/dark cycles and were observed daily to check for survival. Chow containing 4% fat (Harlan Teklad) and water were provided ad libitum. Body weight was recorded every 5 days (Figure 2, B and E) or weekly (Figure 2G). Blood glucose levels were assayed using a Glucometer Elite XL (Bayer). For serum, blood was collected in Vacutainer SST Tubes (BD Biosciences) and centrifuged (1,500 *g* for 15 minutes at 4°C), and serum was stored at –20°C until analysis. Serum hematocrit was analyzed by the Pathology Laboratory of Dallas Children's Medical Center. Total ketone was measured using an Autokit Total Ketone Bodies R1 and R2 Set (Wako Chemicals USA). Total body fat mass was analyzed by NMR using a Minispec mq spectrometer (Bruker). Tissues were harvested and weighed before freezing at –80°C for RNA extraction or

were fixed in 4% paraformaldehyde for paraffin embedding. For histology, 5-μm sections were stained with H&E and analyzed by light microscopy. For fecal nutrient analysis, stools were collected from individually housed mice. Fat content was determined gravimetrically as described (51, 52), and carbohydrate amount was determined by a spectrophotometric method as described (53). Dietary fat absorption was examined by radioactivity of [^{3}H] triolein as described (54). Core body temperature was monitored using Thermalert TH-5 with rectal probes or flexible implantable probes (Physitemp Instruments) between 11:00 and 14:00. For the survival study in a warm environment, 3-week-old mice were housed in a normal environment or on a heating pad (Gaymar Industries) to keep the cage floor at 33°C. For the temperature preference test, the cage was placed on 2 juxtaposed heating pads set at 22°C and 33°C (Mediheat V500 Vstat; Peco Services Ltd.). One of pads was heated at the designated temperature. Mice were videotaped for 1 hour, and the location of the mice was recorded and analyzed every 5 minutes using a TopScan Lite (CleverSys). For the cold environment challenge experiment of constitutive *Et2*-null mice, the body temperature of 6-week-old *Et2*-null mice rescued by a warm environment was monitored. For blood gas analysis, blood was drawn from the retro-orbital plexus into lithium-heparin–coated capillary tubes (Instrumentation Laboratory) and analyzed with a STAT profile Critical Care Xpress (Nova Biomedical). Real-time oxygen saturation percentage of arterial hemoglobin was measured by MouseOx (STARR Life Sciences Corp.) according to the manufacturer's instructions. Serum erythropoietin was assayed using the mouse/rat Quantikine Immunoassay Kit (R&D Systems). Total lung capacity was measured using a flexiVent ventilator and software (Scireq USA) and normalized to body weight. The preparation of epithelial and mesenchymal cell fractions was performed as described (55).

qRT-PCR analysis. Total RNA was extracted from tissues using STAT 60 (Tel-Test), treated with RNase-free DNase I (Roche Molecular Biochemicals), and reverse-transcribed into cDNA with random hexamers (Roche Molecular Biochemicals) and the SuperScript II First-Strand Synthesis System (Invitrogen). Real-time PCR reactions contained 25 ng of cDNA, 150 nM of each primer, and 10 μl of SYBR Green PCR Master Mix (Applied Biosystems) in 20 μl of total volume and were performed with an ABI Prism 7000 Sequence Detection System. Relative mRNA levels were calculated with a ddC_T method normalized to 18s rRNA levels. Primer sequences were designed using Primer Express software (PerkinElmer Life Sciences), and all sequences are available as supplemental material (Supplemental Table 2).

In situ hybridization. A 0.45-kb segment of the mouse *Et2* gene was PCR amplified using 5′-TTTGAATTCAGGCTCCTGCTGCTGTGT-3′ and 5′-TTTCTCGAGGCATGTTCATTTGTCCTC-3′ as primers and cloned into pBluescript II SK (+/–). Sense and antisense riboprobes were generated with T3 and T7 polymerases, respectively, using the Maxiscript kit (Ambion) in the presence of ^{35}S-CTP and -UTP (GE Healthcare). Paraffin-embedded sections were prepared from the tissues of WT control and *Et2*-null mice. Following prehybridization, sections were hybridized at 70°C with sense and antisense riboprobes. Following overnight incubation, unhybridized probe was removed with stringent washes and treatment with RNase A. Slides were subsequently coated with K.5 nuclear emulsion, exposed at 4°C for 4 to 5 weeks, developed, counterstained with hematoxylin, and examined using bright- and dark-field optics.

Statistics. Values are presented as the means ± SEM. Statistical significance was evaluated by conducting a 2-tailed unpaired Student's *t* test using Prism 5.0 (GraphPad Software). A *P* value of less than 0.05 was regarded as statistically significant.

Study approval. All animal experiments were approved by the Institutional Animal Care and Research Advisory Committee of the University of Texas Southwestern Medical Center.

Acknowledgments

We thank Jeremy Nathans (Johns Hopkins University, Baltimore, Maryland, USA) for providing the *Et2$^{f/f}$* mice, and Amber Skach and Randal Floyd for technical support. This work was supported by grants from the Perot Family Foundation, the Exploratory Research for Advanced Technology Japan Science and Technology Agency, and the Japan Society for the Promotion of Science (JSPS) through the Funding Program for World-Leading Innovative R&D on Science and Technology (FIRST), initiated by the Council for Science and Technology Policy (CSTP) (to M. Yanagisawa); and from the Foundation for Fighting Blindness, the Canadian Institutes of Health Research (MOP-7315 and IOP-54037), the Canadian Genetic Diseases Network, and the Macula Vision Research Foundation (to R.R. McInnes). M. Yanagisawa is an Investigator of the Howard Hughes Medical Institute and R.R. McInnes holds a Canada Research Chair.

Received for publication September 5, 2012, and accepted in revised form March 5, 2013.

Address correspondence to: Masashi Yanagisawa, Department of Molecular Genetics and Howard Hughes Medical Institute, The University of Texas Southwestern Medical Center, 5323 Harry Hines Blvd., Dallas, Texas 75390-8584, USA. Phone: 214.648.5082; Fax: 214.648.5068; E-mail: masashi.yanagisawa@utsouthwestern.edu.

Inik Chang's present address is: Urology Research Center, San Francisco Veterans Affairs Medical Center and UCSF, San Francisco, California, USA.

1. Kedzierski RM, Yanagisawa M. Endothelin system: the double-edged sword in health and disease. *Annu Rev Pharmacol Toxicol*. 2001;41:851–876.
2. Kurihara Y, et al. Elevated blood pressure and craniofacial abnormalities in mice deficient in endothelin-1. *Nature*. 1994;368(6473):703–710.
3. Clouthier DE, et al. Cranial and cardiac neural crest defects in endothelin-A receptor-deficient mice. *Development*. 1998;125(5):813–824.
4. Baynash AG, et al. Interaction of endothelin-3 with endothelin-B receptor is essential for development of epidermal melanocytes and enteric neurons. *Cell*. 1994;79(7):1277–1285.
5. Hosoda K, et al. Targeted and natural (piebald-lethal) mutations of endothelin-B receptor gene produce megacolon associated with spotted coat color in mice. *Cell*. 1994;79(7):1267–1276.
6. Rodriguiz RM, et al. Animals lacking endothelin-converting enzyme-2 are deficient in learning and memory. *Genes Brain Behav*. 2008;7(4):418–426.
7. Yanagisawa H, et al. Disruption of ECE-1 and ECE-2 reveals a role for endothelin-converting enzyme-2 in murine cardiac development. *J Clin Invest*. 2000; 105(10):1373–1382.
8. Shohet RV, Kisanuki YY, Zhao XS, Siddiquee Z, Franco F, Yanagisawa M. Mice with cardiomyocyte-specific disruption of the endothelin-1 gene are resistant to hyperthyroid cardiac hypertrophy. *Proc Natl Acad Sci U S A*. 2004;101(7):2088–2093.
9. Kedzierski RM, et al. Cardiomyocyte-specific endothelin A receptor knockout mice have normal cardiac function and an unaltered hypertrophic response to angiotensin II and isoproterenol. *Mol Cell Biol*. 2003;23(22):8226–8232.
10. Ahn D, et al. Collecting duct-specific knockout of endothelin-1 causes hypertension and sodium retention. *J Clin Invest*. 2004;114(4):504–511.
11. Ge Y, Stricklett PK, Hughes AK, Yanagisawa M, Kohan DE. Collecting duct-specific knockout of the endothelin A receptor alters renal vasopressin responsiveness, but not sodium excretion or blood pressure. *Am J Physiol Renal Physiol*. 2005; 289(4):F692–F698.
12. Ge Y, et al. Collecting duct-specific knockout of the endothelin B receptor causes hypertension and sodium retention. *Am J Physiol Renal Physiol*. 2006; 291(6):F1274–F1280.
13. Ge Y, Bagnall A, Stricklett PK, Webb D, Kotelevtsev Y, Kohan DE. Combined knockout of collecting duct endothelin A and B receptors causes hypertension and sodium retention. *Am J Physiol Renal Physiol*. 2008;295(6):F1635–F1640.
14. Bianchi M, Adur J, Takizawa S, Saida K, Casco VH. Endothelin system in intestinal villi: A possible role of endothelin-2/vasoactive intestinal contractor in the maintenance of intestinal architecture. *Biochem Biophys Res Commun*. 2012;417(4):1113–1118.
15. Rattner A, Nathans J. The genomic response to retinal disease and injury: evidence for endothelin signaling from photoreceptors to glia. *J Neurosci*.

2005;25(18):4540–4549.
16. Howell GR, et al. Molecular clustering identifies complement and endothelin induction as early events in a mouse model of glaucoma. *J Clin Invest*. 2011;121(4):1429–1444.
17. Ko C, et al. Endothelin-2 in ovarian follicle rupture. *Endocrinology*. 2006;147(4):1770–1779.
18. Zuidervaart W, et al. Gene expression profiling identifies tumour markers potentially playing a role in uveal melanoma development. *Br J Cancer*. 2003; 89(10):1914–1919.
19. Koong AC, et al. Candidate genes for the hypoxic tumor phenotype. *Cancer Res*. 2000;60(4):883–887.
20. Grimshaw MJ, Wilson JL, Balkwill FR. Endothelin-2 is a macrophage chemoattractant: implications for macrophage distribution in tumors. *Eur J Immunol*. 2002;32(9):2393–2400.
21. Grimshaw MJ, Hagemann T, Ayhan A, Gillett CE, Binder C, Balkwill FR. A role for endothelin-2 and its receptors in breast tumor cell invasion. *Cancer Res*. 2004;64(7):2461–2468.
22. Grimshaw MJ, Naylor S, Balkwill FR. Endothelin-2 is a hypoxia-induced autocrine survival factor for breast tumor cells. *Mol Cancer Ther*. 2002; 1(14):1273–1281.
23. Bot BM, et al. Expression of endothelin 2 and localized clear cell renal cell carcinoma. *Hum Pathol*. 2012; 43(6):843–849.
24. Uchide T, Masuda H, Mitsui Y, Saida K. Gene expression of vasoactive intestinal contractor/endothelin-2 in ovary, uterus and embryo: comprehensive gene expression profiles of the endothelin ligand-receptor system revealed by semi-quantitative reverse transcription-polymerase chain reaction analysis in adult mouse tissues and during late embryonic development. *J Mol Endocrinol*. 1999;22(2):161–171.
25. Hayashi S, McMahon AP. Efficient recombination in diverse tissues by a tamoxifen-inducible form of Cre: a tool for temporally regulated gene activation/inactivation in the mouse. *Dev Biol*. 2002;244(2):305–318.
26. Inagaki T, et al. Endocrine regulation of the fasting response by PPARalpha-mediated induction of fibroblast growth factor 21. *Cell Metab*. 2007; 5(6):415–425.
27. Madison BB, Dunbar L, Qiao XT, Braunstein K, Braunstein E, Gumucio DL. Cis elements of the villin gene control expression in restricted domains of the vertical (crypt) and horizontal (duodenum, cecum) axes of the intestine. *J Biol Chem*. 2002; 277(36):33275–33283.
28. Silva JE, Larsen PR. Adrenergic activation of triiodothyronine production in brown adipose tissue. *Nature*. 1983;305(5936):712–713.
29. Guerra C, Roncero C, Porras A, Fernandez M, Benito M. Triiodothyronine induces the transcription of the uncoupling protein gene and stabilizes its mRNA in fetal rat brown adipocyte primary cultures. *J Biol Chem*. 1996;271(4):2076–2081.
30. Silva JE. Thyroid hormone control of thermogenesis and energy balance. *Thyroid*. 1995;5(6):481–492.
31. Uchide T, et al. Expression of endothelin-1 and vasoactive intestinal contractor genes in mouse organs during the perinatal period. *Clin Sci (Lond)*. 2002;103(suppl 48):167S–170S.
32. Bertin G, Poujeol C, Rubera I, Poujeol P, Tauc M. In vivo Cre/loxP mediated recombination in mouse Clara cells. *Transgenic Res*. 2005;14(5):645–654.
33. Perl AK, Tichelaar JW, Whitsett JA. Conditional gene expression in the respiratory epithelium of the mouse. *Transgenic Res*. 2002;11(1):21–29.
34. Gavrilova O, et al. Torpor in mice is induced by both leptin-dependent and -independent mechanisms. *Proc Natl Acad Sci U S A*. 1999;96(25):14623–14628.
35. Maritz GS, Morley CJ, Harding R. Early developmental origins of impaired lung structure and function. *Early Hum Dev*. 2005;81(9):763–771.
36. Das RM. The effects of intermittent starvation on lung development in suckling rats. *Am J Pathol*. 1984;117(2):326–332.
37. Massaro D, Massaro GD, Baras A, Hoffman EP, Clerch LB. Calorie-related rapid onset of alveolar loss, regeneration, and changes in mouse lung gene expression. *Am J Physiol Lung Cell Mol Physiol*. 2004; 286(5):L896–L906.
38. Bostrom H, et al. PDGF-A signaling is a critical event in lung alveolar myofibroblast development and alveogenesis. *Cell*. 1996;85(6):863–873.
39. Wang X, et al. Dysregulation of TGF-beta1 receptor activation leads to abnormal lung development and emphysema-like phenotype in core fucose-deficient mice. *Proc Natl Acad Sci U S A*. 2005; 102(44):15791–15796.
40. Wilson DO, Donahoe M, Rogers RM, Pennock BE. Metabolic rate and weight loss in chronic obstructive lung disease. *JPEN J Parenter Enteral Nutr*. 1990; 14(1):7–11.
41. Kozak W, Wrotek S, Walentynowicz K. Hypoxia-induced sickness behaviour. *J Physiol Pharmacol*. 2006;57(suppl 8):35–50.
42. Wood SC. Interactions between hypoxia and hypothermia. *Annu Rev Physiol*. 1991;53:71–85.
43. Schaefer KE, Messier AA, Morgan C, Baker GT. Effect of chronic hypercapnia on body temperature regulation. *J Appl Physiol*. 1975;38(5):900–906.
44. Andrews MT, Squire TL, Bowen CM, Rollins MB. Low-temperature carbon utilization is regulated by novel gene activity in the heart of a hibernating mammal. *Proc Natl Acad Sci U S A*. 1998; 95(14):8392–8397.
45. Zhang J, Kaasik K, Blackburn MR, Lee CC. Constant darkness is a circadian metabolic signal in mammals. *Nature*. 2006;439(7074):340–343.
46. Ling L, Maguire JJ, Davenport AP. Endothelin-2, the forgotten isoform: emerging role in the cardiovascular system, ovarian development, immunology and cancer. *Br J Pharmacol*. 2013;168(2):283–295.
47. Hogaboam CM, Muller MJ, Collins SM, Hunt RH. An orally active non-selective endothelin receptor antagonist, bosentan, markedly reduces injury in a rat model of colitis. *Eur J Pharmacol*. 1996; 309(3):261–269.
48. Gulluoglu BM, et al. Role of endothelins in trinitrobenzene sulfonic acid-induced colitis in rats. *Digestion*. 1999;60(5):484–492.
49. Padol I, Huang JQ, Hogaboam CM, Hunt RH. Therapeutic effects of the endothelin receptor antagonist Ro 48-5695 in the TNBS/DNBS rat model of colitis. *Eur J Gastroenterol Hepatol*. 2000;12(3):257–265.
50. McCartney SA, Ballinger AB, Vojnovic I, Farthing MJ, Warner TD. Endothelin in human inflammatory bowel disease: comparison to rat trinitrobenzenesulphonic acid-induced colitis. *Life Sci*. 2002; 71(16):1893–1904.
51. Folch J, Lees M, Sloane Stanley GH. A simple method for the isolation and purification of total lipides from animal tissues. *J Biol Chem*. 1957;226(1):497–509.
52. Schwarz M, et al. Disruption of cholesterol 7alpha-hydroxylase gene in mice. II. Bile acid deficiency is overcome by induction of oxysterol 7alpha-hydroxylase. *J Biol Chem*. 1996;271(30):18024–18031.
53. Ameen VZ, Powell GK. A simple spectrophotometric method for quantitative fecal carbohydrate measurement. *Clin Chim Acta*. 1985;152(1–2):3–9.
54. Oishi K, et al. Disrupted fat absorption attenuates obesity induced by a high-fat diet in Clock mutant mice. *FEBS Lett*. 2006;580(1):127–130.
55. Caniggia I, Tseu I, Han RN, Smith BT, Tanswell K, Post M. Spatial and temporal differences in fibroblast behavior in fetal rat lung. *Am J Physiol*. 1991; 261(6 pt 1):L424–L433.